Hinkkanen, Marko; Luomi, Jorma

Parameter sensitivity of full-order flux observes for induction motors

Published in:
IEEE Transactions on Industry Applications

DOI:
10.1109/TIA.2003.814560

Published: 28/07/2003

Document Version
Peer-reviewed accepted author manuscript, also known as Final accepted manuscript or Post-print

Please cite the original version:
Hinkkanen, M., & Luomi, J. (2003). Parameter sensitivity of full-order flux observes for induction motors. *IEEE Transactions on Industry Applications*, *33*(4), 1127-1135. https://doi.org/10.1109/TIA.2003.814560

Parameter Sensitivity of Full-Order Flux Observers for Induction Motors

Marko Hinkkanen and Jorma Luomi

***Abstract*— This paper deals with flux estimation for induction motor drives. The equations of the parameter sensitivity of both the rotor flux estimation and the torque production are derived for a full-order flux observer. Based on the parameter sensitivity analysis, practical methods of designing robust observer gains combining the current model and the voltage model are proposed. The proposed gains are easy to tune and lead to a simple observer structure. Experimental results show that for inaccurate parameter estimates, both the steady-state and dynamic errors in the produced torque are small as compared to the current model. Furthermore, high-speed operation is possible without modelling the magnetic saturation even if motor parameters are highly erroneous.**

***Index Terms*— Induction motors, full-order flux observer, parameter sensitivity.**

I. Introduction

High-performance field orientation control of induction motors requires flux estimation. A flux estimator is a dynamic model of the motor requiring estimates of motor parameters. A problem is that actual parameters of the motor vary with temperature (resistances) and magnetic saturation (inductances). Inaccurate motor parameters may cause input-output torque nonlinearity and saturation of the motor [1]. Consequently, the flux estimator should be as insensitive to varying parameters as possible. The parameter sensitivity of both the flux estimation and the torque production for the conventional indirect field orientation control was analyzed in [1]. The parameter sensitivities of the usual reduced-order flux observers used in direct field orientation control were compared in [2], and an observer combining the current and voltage models was proposed.

The full-order flux observer [3], [4] is a versatile flux estimator for both speed-sensored and speed-sensorless drives. It offers good performance and robustness against measurement noise. An observer gain determines the properties of the observer. The selection of the observer gain has a major influence on the parameter sensitivity of the observer.

This paper presents the steady-state parameter sensitivity analysis of both the flux estimation and the torque production for rotor flux orientation controlled drives using a full-order flux observer. Based on the analysis, simple methods to determine robust observer gains combining the current model and the voltage model behavior are proposed. The observer using the proposed gain is studied by means of analysis and experiments.

II. Induction Motor Model

The parameters of the dynamic inverse-Γ-equivalent circuit of an induction motor are the stator resistance R_s, the rotor resistance R_R, the stator transient inductance L'_s, and the magnetizing inductance L_M. The electrical angular speed of the rotor is denoted by ω_m, the angular speed of the reference frame ω_k, the stator current space vector $\underline{i}_s$, and the stator voltage $\underline{u}_s$. When the stator flux $\underline{\psi}_s$ and the rotor flux $\underline{\psi}_R$ are chosen as state variables, the state-space representation of the induction motor becomes

$$\dot{\underline{\mathbf{x}}} = \underbrace{\begin{bmatrix} -\frac{1}{\tau'_s} - j\omega_k & \frac{1}{\tau'_s} \\ \frac{1-\sigma}{\tau'_r} & -\frac{1}{\tau'_r} - j\left(\omega_k - \omega_m\right) \end{bmatrix}}_{\mathbf{A}} \underline{\mathbf{x}} + \underbrace{\begin{bmatrix} 1 \\ 0 \end{bmatrix}}_{\mathbf{B}} \underline{u}_s \tag{1a}$$

$$\underline{i}_s = \underbrace{\begin{bmatrix} \frac{1}{L'_s} & -\frac{1}{L'_s} \end{bmatrix}}_{\mathbf{C}} \underline{\mathbf{x}} \tag{1b}$$

where the state vector is $\underline{\mathbf{x}} = [\underline{\psi}_s \quad \underline{\psi}_R]^T$, and the parameters are $\sigma = L'_s/(L_M + L'_s)$, $\tau'_s = L'_s/R_s$, and $\tau'_r = \sigma L_M/R_R$. The electromagnetic torque is

$$T_e = \frac{3}{2} p \operatorname{Im}\left\{\underline{i}_s \underline{\psi}_s^*\right\} = \frac{3}{2} p \frac{1}{L'_s} \operatorname{Im}\left\{\underline{\psi}_s \underline{\psi}_R^*\right\} \tag{2}$$

where p is the number of pole pairs and the complex conjugate is marked by the symbol *.

III. Full-Order Flux Observer

A. General Reference Frame

Conventionally, the stator current and the rotor flux are used as state variables in full-order flux observers. However, choosing the stator and rotor fluxes as state variables is preferred since no inductance derivatives are needed and the modelling of magnetic saturation becomes simpler. In addition, the observer could be used with stator flux orientation control or direct torque control [5] as well as with rotor flux orientation control. The full-order flux observer using the fluxes as state variables is defined by

$$\dot{\hat{\underline{\mathbf{x}}}} = \hat{\underline{\mathbf{A}}}\,\hat{\underline{\mathbf{x}}} + \mathbf{B}\underline{u}_s + \underline{\mathbf{L}}(\underline{i}_s - \hat{\underline{i}}_s) \tag{3a}$$

$$\hat{\underline{i}}_s = \hat{\mathbf{C}}\hat{\underline{\mathbf{x}}} \tag{3b}$$

where the observer state vector is $\hat{\underline{\mathbf{x}}} = [\hat{\underline{\psi}}_s \quad \hat{\underline{\psi}}_R]^T$, and the system matrix and the observer gain are

$$\hat{\underline{\mathbf{A}}} = \begin{bmatrix} -\frac{1}{\hat{\tau}'_s} - j\omega_k & \frac{1}{\hat{\tau}'_s} \\ \frac{1-\hat{\sigma}}{\hat{\tau}'_r} & -\frac{1}{\hat{\tau}'_r} - j(\omega_k - \omega_m) \end{bmatrix}, \quad \underline{\mathbf{L}} = \begin{bmatrix} \underline{l}_s \\ \underline{l}_r \end{bmatrix} \tag{3c}$$

respectively, where the estimates are marked by the symbol $\hat{}$.

B. Implementation in the Estimated Flux Reference Frame

The reference frame of the observer (3) can be selected freely. The full-order flux observers are often implemented in the stator reference frame, i.e., $\omega_k = 0$ (direct rotor flux orientation). The observer can also be implemented in the estimated rotor flux reference frame, i.e., $\underline{\hat{\psi}}_R = \hat{\psi}_R + j0$ and $\omega_k = \hat{\omega}_s$, where $\hat{\omega}_s$ is the angular speed of the estimated rotor flux. The observer (3) divided into components in the selected reference frame becomes

$$\dot{\hat{\psi}}_{sd} = -\tfrac{1}{\hat{\tau}'_s}\hat{\psi}_{sd} + \hat{\omega}_s\hat{\psi}_{sq} + \tfrac{1}{\hat{\tau}'_s}\hat{\psi}_R + u_{sd} + l_{sd}\tilde{i}_{sd} - l_{sq}\tilde{i}_{sq} \quad (4a)$$

$$\dot{\hat{\psi}}_{sq} = -\hat{\omega}_s\hat{\psi}_{sd} - \tfrac{1}{\hat{\tau}'_s}\hat{\psi}_{sq} + u_{sq} + l_{sd}\tilde{i}_{sq} + l_{sq}\tilde{i}_{sd} \quad (4b)$$

$$\dot{\hat{\psi}}_R = \tfrac{1-\hat{\sigma}}{\hat{\tau}'_r}\hat{\psi}_{sd} - \tfrac{1}{\hat{\tau}'_r}\hat{\psi}_R + l_{rd}\tilde{i}_{sd} - l_{rq}\tilde{i}_{sq} \quad (4c)$$

where

$$\tilde{i}_{sd} = i_{sd} - \hat{i}_{sd} = i_{sd} - \frac{\hat{\psi}_{sd} - \hat{\psi}_R}{\hat{L}'_s} \quad (4d)$$

$$\tilde{i}_{sq} = i_{sq} - \hat{i}_{sq} = i_{sq} - \frac{\hat{\psi}_{sq}}{\hat{L}'_s} \quad (4e)$$

and the entries of the observer gain are divided into real and imaginary components: $\underline{l}_s = l_{sd} + jl_{sq}$ and $\underline{l}_r = l_{rd} + jl_{rq}$. The angular speed of the estimated rotor flux is solved from (3) by using the fact that the imaginary component of $\underline{\hat{\psi}}_R$ is zero:

$$\hat{\omega}_s = \omega_m + \frac{\frac{1-\hat{\sigma}}{\hat{\tau}'_r}\hat{\psi}_{sq} + l_{rd}\tilde{i}_{sq} + l_{rq}\tilde{i}_{sd}}{\hat{\psi}_R} \quad (4f)$$

and the angle $\hat{\vartheta}_s$ of the estimated flux is obtained simply by integrating $\hat{\omega}_s$. It is worth noting that the implementation (4) of the observer resembles the conventional indirect rotor flux orientation, see also [6]. A computationally efficient digital implementation of (4) is given in the Appendix.

IV. Parameter Sensitivity Analysis

A. Steady State

1) Flux Estimation: The parameter sensitivity of the flux observers can be analyzed by means of the steady-state expression for $\underline{\hat{\psi}}_R/\underline{\psi}_R$ [2]. The following steady-state relations are obtained by inserting $d/(dt) = 0$ and $\omega_k = \omega_s$ into (1) and (3), where ω_s is the angular stator frequency. The relation between the stator voltage and the stator current is

$$\underline{i}_s = \frac{\tau'_s}{L'_s}\frac{\sigma + j\omega_r\tau'_r}{\sigma - \omega_s\omega_r\tau'_s\tau'_r + j\left(\omega_s\tau'_s + \omega_r\tau'_r\right)}\underline{u}_s \quad (5)$$

and between the stator voltage and the rotor flux

$$\underline{\psi}_R = \frac{\left(1-\sigma\right)\tau'_s}{\sigma - \omega_s\omega_r\tau'_s\tau'_r + j\left(\omega_s\tau'_s + \omega_r\tau'_r\right)}\underline{u}_s \quad (6)$$

where the angular slip frequency is $\omega_r = \omega_s - \omega_m$. The expression for the estimated rotor flux is given in (7). The desired relation $\underline{\hat{\psi}}_R/\underline{\psi}_R$ is obtained by inserting (5) into (7) and then dividing both sides of (7) by (6). Relations for other estimators and observers as well as comparisons of various observers can be found in [7]–[9].

The relation $\underline{\hat{\psi}}_R/\underline{\psi}_R$ can also be used in the case of speed-sensorless drives, where the observer (3) is augmented with a speed-adaptation law. The slip frequency ω_r in (7) should be replaced with its estimate $\hat{\omega}_r = \omega_s - \hat{\omega}_m$, where the speed estimate $\hat{\omega}_m$ is a steady-state solution of the speed-adaptation law and can be obtained, e.g., by using iteration [10].

It is interesting to consider two important flux estimators, the current model and the voltage model, as two special cases of the full-order flux observer (3). A real-valued observer gain is considered, i.e., $\underline{l}_s = l_s$ and $\underline{l}_r = l_r$. The current model is obtained by choosing the observer gain

$$l_s \geq -\hat{R}_s = -\frac{\hat{L}'_s}{\hat{\tau}'_s}, \quad l_r = \hat{R}_R = \frac{(1-\hat{\sigma})\hat{L}'_s}{\hat{\tau}'_r} \quad (8)$$

yielding the relation

$$\frac{\underline{\hat{\psi}}_R}{\underline{\psi}_R} = \frac{\hat{L}_M}{L_M}\frac{1 + j\omega_r\tau_r}{1 + j\omega_r\hat{\tau}_r} \quad (9)$$

where the rotor time constant is $\tau_r = L_M/R_R$. Equation (9) equals to the result given in [2] for the current model. The voltage model behavior is obtained by choosing

$$l_s = -\hat{R}_s, \quad l_r \to -\infty \quad (10)$$

where the sign of l_r is chosen according to stability conditions. In practice, it is sufficient to choose l_r considerably smaller than l_s. In order to avoid pure integration, l_s should be chosen slightly larger than $-\hat{R}_s$. Equation (10) leads to the relation

$$\frac{\underline{\hat{\psi}}_R}{\underline{\psi}_R} = 1 + \frac{1 + j\omega_r\tau_r}{L_M}\left(L'_s - \hat{L}'_s - j\frac{R_s - \hat{R}_s}{\omega_s}\right) \quad (11)$$

which equals to the result given in [2] for the voltage model.

2) Torque Production: If the drive is operated in the torque mode, i.e., the speed-control loop is disabled, the accuracy of the produced torque is crucial. Parameter sensitivities of the flux estimation and torque production are closely related as will be shown. A typical rotor flux orientation control scheme is shown in Fig. 1. The magnitude of the rotor flux estimate is controlled by using a flux controller, and the angle of the flux estimate is used in the coordinate transformation. Consequently, the reference of the rotor flux is $\underline{\psi}_{R,ref} = \underline{\hat{\psi}}_R$ in the steady state. In the following, the d-axis of the reference frame is fixed to the actual rotor flux of the motor as shown in Fig. 2. The actual flux is real, i.e., $\underline{\psi}_R = \psi_R$. The flux estimate can be written as

$$\underline{\hat{\psi}}_R = \hat{\psi}_{Rd} + j\hat{\psi}_{Rq} = \hat{\psi}_R e^{j\vartheta} \quad (12)$$

where $\vartheta = \angle(\underline{\hat{\psi}}_R/\underline{\psi}_R) = \angle\underline{\hat{\psi}}_R - \angle\underline{\psi}_R$ is the angle between the estimated flux and the actual flux. If the current regulation is assumed to be ideal, the reference torque is

$$\begin{aligned} T_{e,ref} &= \frac{3}{2}p(\hat{\psi}_{Rd}i_{sq} - \hat{\psi}_{Rq}i_{sd}) \\ &= \frac{3}{2}p\hat{\psi}_R(i_{sq}\cos\vartheta - i_{sd}\sin\vartheta) \end{aligned} \quad (13)$$

and the actual torque is $T_e = \frac{3}{2}p\psi_R i_{sq}$, yielding

$$\frac{T_{e,ref}}{T_e} = \left|\frac{\underline{\hat{\psi}}_R}{\underline{\psi}_R}\right|\left(\cos\vartheta - \frac{\sin\vartheta}{\omega_r\tau_r}\right) \quad (14)$$

$$\underline{\hat{\psi}}_R = \frac{\hat{\tau}'_s\left(1-\hat{\sigma}-\frac{\hat{\tau}'_r\underline{l}_r}{\hat{L}'_s}\right)\underline{u}_s + \left[(1-\hat{\sigma})\,\hat{\tau}'_s\underline{l}_s + (1+j\omega_s\hat{\tau}'_s)\,\hat{\tau}'_r\underline{l}_r\right]\underline{i}_s}{\hat{\sigma}\left(1+\frac{\hat{\tau}'_s\underline{l}_s}{\hat{L}'_s}\right) - \omega_s\omega_r\hat{\tau}'_s\hat{\tau}'_r + j\omega_s\hat{\tau}'_s\left(1-\frac{\hat{\tau}'_r\underline{l}_r}{\hat{L}'_s}\right) + j\omega_r\hat{\tau}'_r\left(1+\frac{\hat{\tau}'_s\underline{l}_s}{\hat{L}'_s}\right)} \tag{7}$$

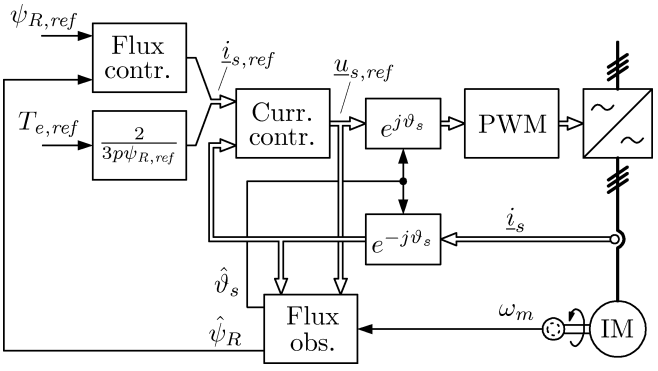

Fig. 1. Rotor flux orientation control. The electrical variables shown on the left-hand side of the coordinate transformations are in the estimated rotor flux reference frame and the variables on the right-hand side are in the stator reference frame. If the observer is implemented in the stator reference frame, the complex-valued inputs of the observer are taken from the right-hand side of the coordinate transformations.

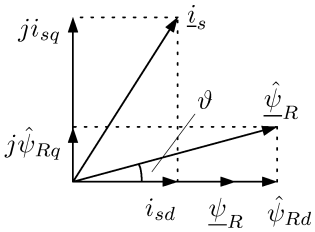

Fig. 2. The actual rotor flux of the motor, the estimated flux, and the stator current.

since $i_{sq}/i_{sd} = \omega_r\tau_r$ in the reference frame of the actual rotor flux. The torque error can thus be easily determined if the relation $\hat{\underline{\psi}}_R/\underline{\psi}_R$ is known. When the observer gain (8) yielding the current model is chosen, the relationship (14) corresponds to the well-known result in [1] derived for the conventional indirect field orientation control (where neither the flux magnitude estimation nor the flux regulator are used). The parameter sensitivity of the torque production of the direct field orientation using the current model is equal to that of the conventional indirect field orientation.

B. Dynamics

The dynamics of the estimation error $\underline{\mathbf{e}} = \underline{\mathbf{x}} - \hat{\underline{\mathbf{x}}}$ of the state vector can be written based on (1) and (3)

$$\dot{\underline{\mathbf{e}}} = \left(\hat{\underline{\mathbf{A}}} - \underline{\mathbf{L}}\hat{\mathbf{C}}\right)\underline{\mathbf{e}} + \Delta\underline{\mathbf{A}}\underline{\mathbf{x}} - \underline{\mathbf{L}}\Delta\mathbf{C}\underline{\mathbf{x}} \tag{15}$$

where the error matrices are $\Delta\underline{\mathbf{A}} = \underline{\mathbf{A}} - \hat{\underline{\mathbf{A}}}$ and $\Delta\mathbf{C} = \mathbf{C} - \hat{\mathbf{C}}$. In practice, dynamic analysis of the system (15) including parameter errors becomes cumbersome. Consequently, the effect of parameter errors on dynamics are studied using computer simulations and experiments.

The rotor speed can be assumed to be constant if the mechanical dynamics are much slower than the electrical dynamics. The dynamics of the system without parameter errors ($\Delta\underline{\mathbf{A}} = 0$, $\Delta\mathbf{C} = 0$) can then be easily analyzed since the system (15) becomes linear.

V. Observer Gain Design

An observer gain can be determined based on the steady-state parameter sensitivity analysis. If presumable parameter errors are small, even a constant real-valued observer gain giving a compromise between the current model and the voltage model may be sufficient. If large parameter variations are assumed to occur, it is reasonable to vary the observer gain as a function of the rotor speed.

At low speeds, the robustness of the current model against inaccurate parameter estimates is better than that of the voltage model, whereas the voltage model is better at high speeds [2]. The observer gain combining the current model and the approximate voltage model can be easily formed based on (8) and (10). This combination can be achieved even if the simple gain component $\underline{l}_s = 0$ is used, leading to

$$\underline{l}_s = 0 \tag{16a}$$

$$\underline{l}_r = \begin{cases} \underline{l}_{r1} & \text{if } |\omega_m| \le \omega_{\Delta1} \\ \frac{l_{r2}-\underline{l}_{r1}}{\omega_{\Delta2}-\omega_{\Delta1}}\left(|\omega_m|-\omega_{\Delta1}\right)+\underline{l}_{r1} & \text{if } \omega_{\Delta1} < |\omega_m| < \omega_{\Delta2} \\ l_{r2} & \text{if } |\omega_m| \ge \omega_{\Delta2} \end{cases} \tag{16b}$$

where the possibly complex-valued parameter $\underline{l}_{r1}$ determines the contribution of the current model at low speeds and the real-valued parameter l_{r2} determines the contribution of the voltage model at higher speeds. Parameters $\omega_{\Delta1}$ and $\omega_{\Delta2}$ determine the transition region between the (possibly approximate) current model and the approximate voltage model.

The stability of the system without parameter errors was studied by analyzing the eigenvalues of $\hat{\underline{\mathbf{A}}} - \underline{\mathbf{L}}\hat{\mathbf{C}}$. Stability is guaranteed by choosing

$$\underline{l}_{r1} = \left[k_d + jk_q\,\mathrm{sign}(\omega_m)\right]\hat{R}_R \tag{16c}$$

where $k_d \le 1$ and $k_q \ge 0$. The selection of the parameters k_d and k_q will be discussed in the following subsections.

In this paper, the motor parameters of a 2.2-kW four-pole induction motor given in Table I are used. The parameters of (16) are $\omega_{\Delta1} = 0.5$ p.u., $\omega_{\Delta2} = 1$ p.u., and $l_{r2} = -\hat{R}_R$. The most widely used flux estimators, the current model and the voltage model, are used as benchmarks for the parameter sensitivity graphs. The proposed observer gain design principles can be applied to any induction motor, but some fine tuning of the parameters of (16) may be needed.

A. Real-Valued Gain

The pure current model behavior at low speeds is obtained by selecting $\underline{l}_{r1} = \hat{R}_R$, leading to the gain components shown

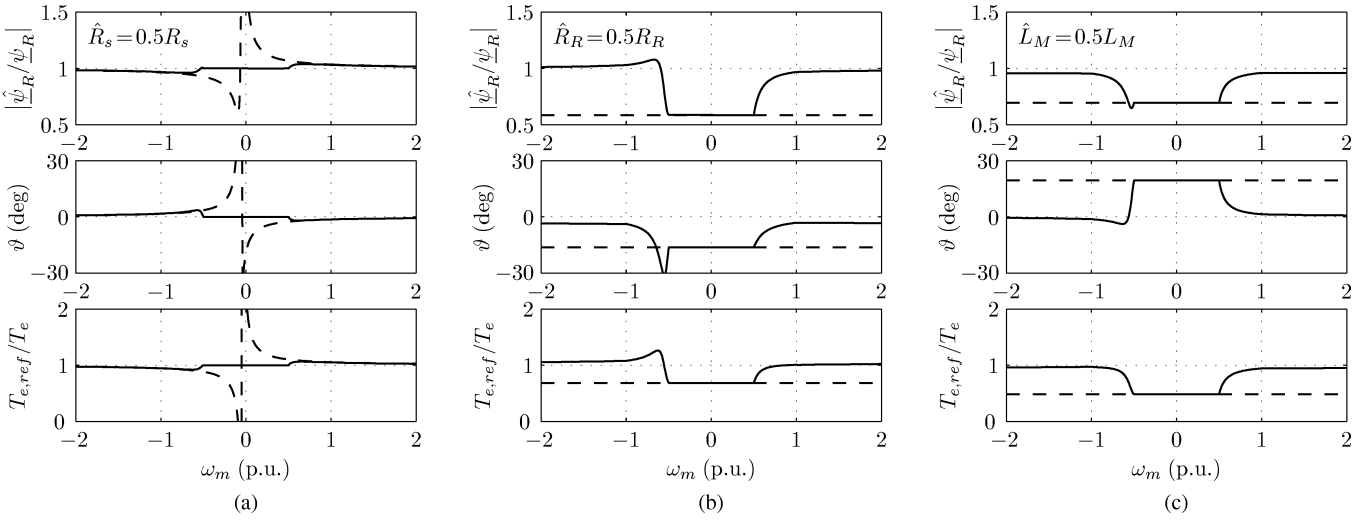

Fig. 4. Parameter sensitivities using the observer gain (16) with $\underline{l}_{r1} = \hat{R}_R$ are shown by the continuous lines: (a) $\hat{R}_s = 0.5R_s$, (b) $\hat{R}_R = 0.5R_R$, (c) $\hat{L}_M = 0.5L_M$. The parameter sensitivities of the voltage model (a) and the current model (b,c) are shown by the dashed line. The slip corresponds to the rated-load torque in perfect field orientation.

TABLE I
PARAMETERS OF THE 2.2-KW FOUR-POLE 400-V 50-HZ MOTOR.

Stator resistance R_s	3.67 Ω
Rotor resistance R_R	2.10 Ω
Stator transient inductance L'_s	0.0209 H
Magnetizing inductance L_M	0.224 H
Total moment of inertia	0.0155 kgm^2
Rated speed	1 430 r/min
Rated current	5.0 A
Rated torque	14.6 Nm

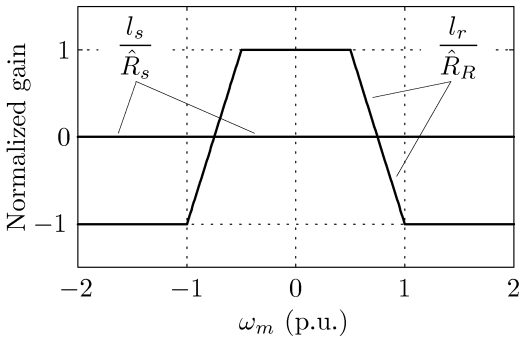

Fig. 3. An example of the observer gain for combining the current model and the approximate voltage model. Real-valued gain components ($\underline{l}_s = l_s = 0$, $\underline{l}_r = l_r$).

in Fig. 3. Fig. 4 shows examples of the parameter sensitivities when the slip frequency corresponds to the rated-load torque in perfect field orientation. It can be seen that the observer is equal to the current model at low speeds, whereas it behaves as an approximate voltage model at high speeds. The full-order flux observer using the real-valued gain has a simple structure and is easy to tune. Sensitivity to the stator transient inductance L'_s is not shown since both the voltage model and the observer using the proposed gain are comparatively insensitive to L'_s.

Even though the parameter sensitivity in the regeneration mode has usually not been studied [2], [7], the regeneration mode operation generally suffers more under erroneous parameters than the motoring mode operation. This can also be seen, e.g., in Fig. 4(b). However, the pure current model is an exception: the steady-state parameter sensitivities in both the regeneration and motoring modes are similar as can be seen from Figs. 4(b,c).

B. Complex-Valued Gain

If some of the stator dynamics are taken into account also at low speeds, sensitivity to the rotor parameters can be reduced without causing too much sensitivity to the stator parameters. In the motoring mode operation, good results are obtained simply selecting $\underline{l}_{r1} < \hat{R}_R$, e.g., $\underline{l}_{r1} = 0.8\hat{R}_R$. However, the regeneration mode operation is more problematic, especially in case of small motors. When $|\omega_m| = 0 \ldots \omega_{\Delta 1}$ in the regeneration mode and $\underline{l}_{r1} < \hat{R}_R$ is selected, the sensitivity to the rotor resistance increases compared to the selection $\underline{l}_{r1} = \hat{R}_R$.

The observer gain is not restricted to be real. The behavior in the regeneration mode can be remedied by means of the imaginary part of the parameter $\underline{l}_{r1}$ in (16c). For the 2.2-kW motor, the parameters $k_d = 0.8$ and $k_q = 0.2$ are suitable: the parameter sensitivity in the regeneration mode decreases and the motoring mode behavior remains approximately same as without the imaginary part. The parameter sensitivity graphs are shown in Fig. 5. As desired, the sensitivity to the rotor parameters at low speeds is reduced, compared to Fig. 4.

VI. CONTROL SYSTEM

The observer using the proposed gain (16) with $k_d = 0.8$ and $k_q = 0.2$ was investigated experimentally, using the current model as a benchmark. The control system was based on rotor flux orientation. The system shown in Fig. 1 was supplemented with a speed controller in some experiments. The digital implementation of the observer is given in the

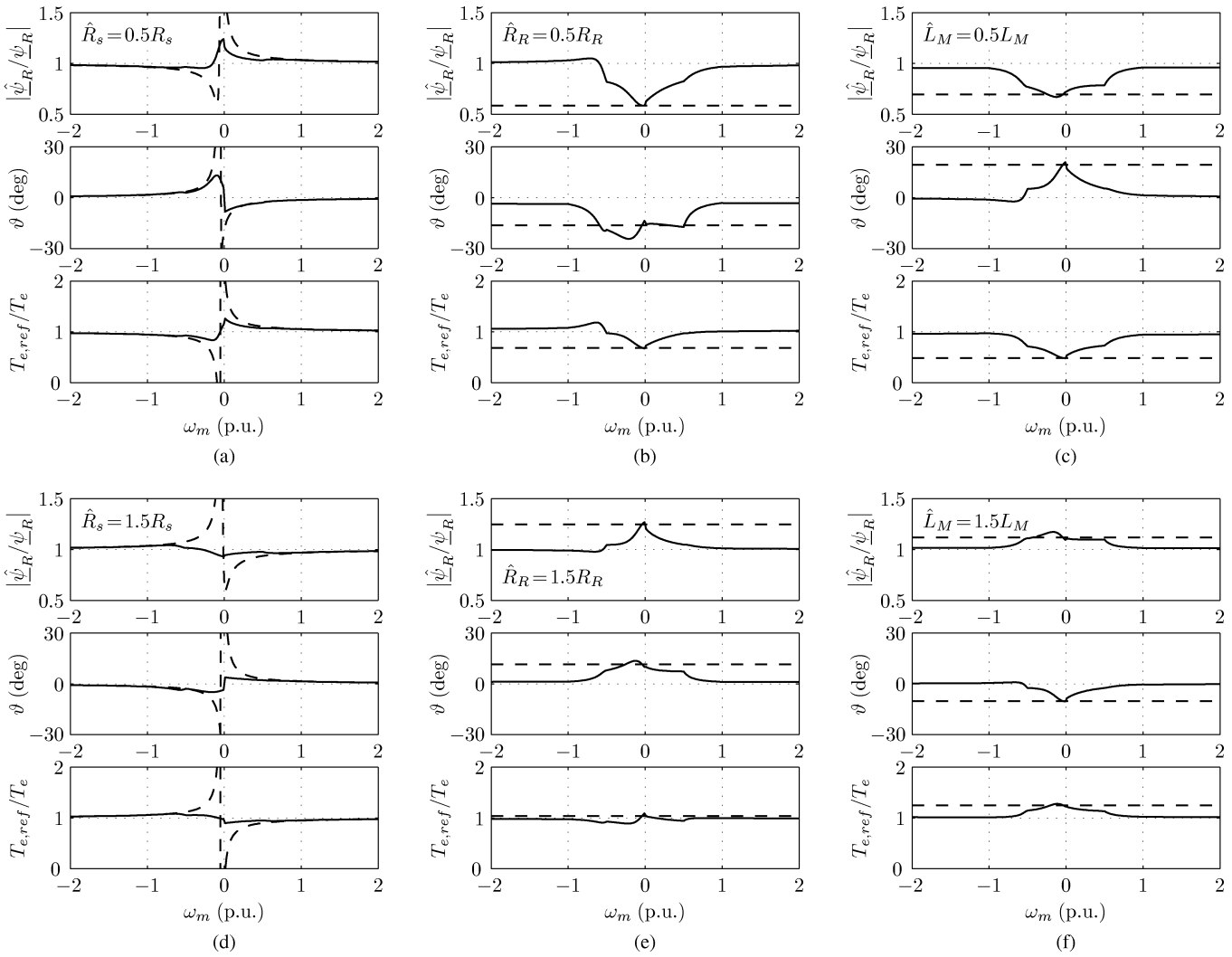

Fig. 5. Parameter sensitivities using the observer gain (16) with $k_d = 0.8$, $k_q = 0.2$ are shown by the continuous lines: (a) $\hat{R}_s = 0.5R_s$, (b) $\hat{R}_R = 0.5R_R$, (c) $\hat{L}_M = 0.5L_M$, (d) $\hat{R}_s = 1.5R_s$, (e) $\hat{R}_R = 1.5R_R$, (f) $\hat{L}_M = 1.5L_M$. The parameter sensitivities of the voltage model (a,d) and the current model (b,c,e,f) are shown by the dashed line. The slip corresponds to the rated-load torque in perfect field orientation.

Appendix. The base values are: angular speed $2\pi \cdot 50$ s^{-1}, current $\sqrt{2} \cdot 5.0$ A, flux 1.04 Wb, and torque 21.4 Nm.

A PI-type synchronous-frame current controller [11], [12] including the decoupling of the back-emf voltages was used. The bandwidth of the current controller was 8 p.u. The speed controller was a conventional PI-controller having the bandwidth of 0.24 p.u. The flux controller was a PI-type controller including a feedforward path [13]. The bandwidth of both the feedforward path and the feedback loop of the flux controller was 0.08 p.u. The conventional $1/\omega_m$-field-weakening scheme was used. The slip was limited to the pull-out slip at very high speeds. The field-weakening point was at the rotor speed 0.85 p.u. and the rotor flux in the base-speed region was 0.87 p.u. The magnitude of the stator current was limited to 1.5 p.u.

The sampling was synchronized to the modulation, and both the switching frequency and the sampling frequency were 5 kHz. The dc-link voltage was measured, and the reference stator voltage obtained from the current controller was used for the flux observer. Constant-valued motor parameters were used, the value of $\hat{L}_M$ corresponding to the base-speed region.

VII. Experimental Results

The experimental setup is shown in Fig. 6. The 2.2-kW four-pole induction motor (Table I) was fed by a frequency converter controlled by a dSpace DS1103 PPC/DSP board. The measured rotor speed was used as feedback signal for the control. The shaft torque measured using a HBM T10F torque flange was used only for monitoring.

A. Steady State

A sufficiently slow speed reversal can be considered as steady-state operation from the flux observer's point of view. The steady-state behavior of the observer was studied using the torque mode control, the torque reference being set to the rated torque. The speed of the rotor was ramped from -1 p.u. to 1 p.u. in one minute using the loading machine. The reference torque $T_{e,ref}$ is compared to the measured shaft torque T_m.

An example of the experimental waveforms obtained using the full-order observer and measured parameters is shown in

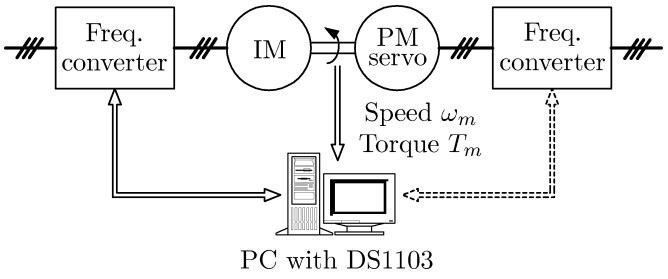

Fig. 6. The experimental setup. The PM servo motor was used as loading machine. The measured shaft torque T_m was used only for monitoring.

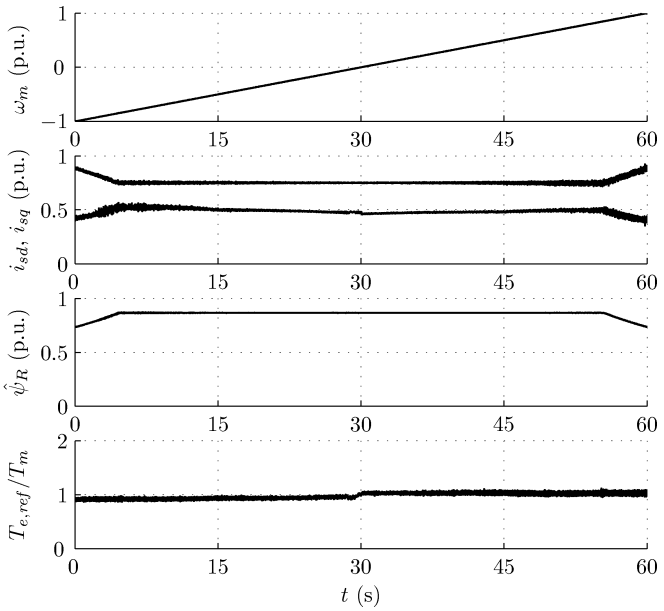

Fig. 7. Experimental results showing steady-state operation in the torque mode. The observer using the proposed gain and the measured motor parameters is used. The first subplot shows the measured speed. The second subplot shows the d (lower) and q (upper) components of the stator current in the estimated rotor flux reference frame. The third subplot presents the magnitude of the estimated rotor flux. The last subplot shows the reference torque divided by the measured shaft torque.

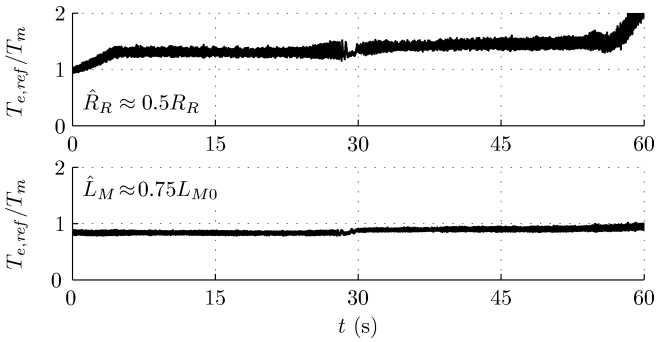

Fig. 8. Experimental results showing the ratio of the reference torque to the measured torque for the current model under erroneous parameters. The measurement was similar to that of Fig. 7. The magnetizing inductance L_{M0} is the measured value corresponding to the base-speed region.

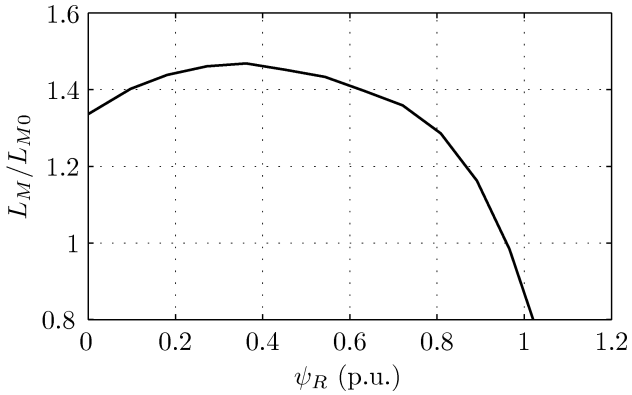

Fig. 9. Measured magnetizing inductance of the 2.2-kW motor. The base value of the flux is 1.04 Wb and $L_{M0} = 0.224$ H.

Fig. 7. Since the mechanical losses are not compensated, there is a small difference in the measured shaft torque between the motoring and regeneration modes. The results for the current model with measured parameters are similar to Fig. 7.

Fig. 8 shows the ratio of the reference torque to the measured shaft torque for the current model under erroneous parameters. The results differ from the parameter sensitivity graphs shown by the dashed lines in Figs. 4(b,c). There are two main causes for the differences between the results of this experiment and the graphs based on the analytical relations. Firstly, the reference torque is kept constant but the slip varies according to the parameter errors. The parameter sensitivity graphs correspond to the constant slip. Secondly, due to magnetic saturation, the estimate of the magnetizing inductance $\hat{L}_M$ may become highly erroneous due to the errors in other parameters. The measured magnetizing curve of the 2.2-kW motor as a function of the rotor flux magnitude is depicted in Fig. 9. When the magnitude of the flux is inaccurately estimated, the magnitude of the actual flux does not correspond to its reference (or its estimate). Consequently, the estimate of the magnetizing inductance $\hat{L}_M$ becomes erroneous (even if the magnetizing curve would be accurately modelled).

In the first subplot of Fig. 8, the slip in the base-speed region is half of the value corresponding to the perfect field orientation due to $\hat{R}_R \approx 0.5R_R$. The actual flux is larger than its estimate (cf. Fig. 4(b)) and, consequently, the actual magnetizing inductance becomes smaller, i.e., $\hat{L}_M > L_M$. Due to these changes, the produced torque is actually smaller than its reference. This can also be verified by using analytical relations.

In the regeneration mode before $t = 5$ s, the slip frequency changes due to the field weakening. The increased slip also makes the produced torque larger in that region. In the motoring mode after $t = 55$ s, the slip would also increase due to the weakened flux but all the available voltage is in use due to incorrect flux estimation (at the same speed, more voltage is required in the motoring mode than in the regeneration mode). Consequently, the actual q-component of the stator current cannot be controlled to its reference, and both the slip and the torque decrease.

In the second subplot of Fig. 8 ($\hat{L}_M \approx 0.75L_M$), the result corresponds better to the parameter sensitivity graphs. The slip in the base-speed region corresponds to the value of the perfect field orientation. However, the actual flux is larger than its estimate and, consequently, the actual magnetizing inductance

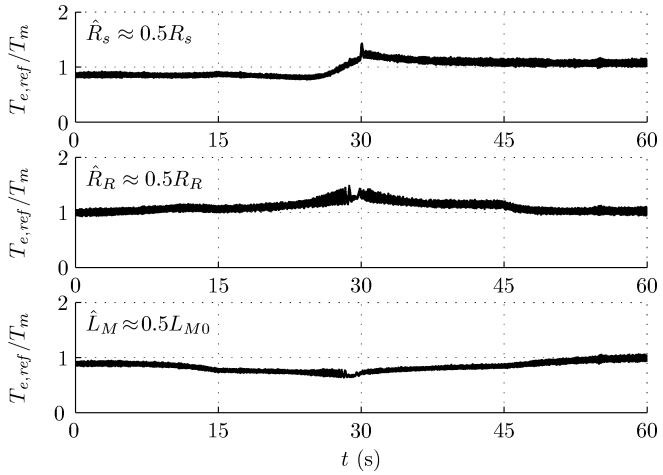

Fig. 10. Experimental results showing the ratio of the reference torque to the measured torque for the full-order flux observer under erroneous parameters. The measurement was similar to that of Fig. 7.

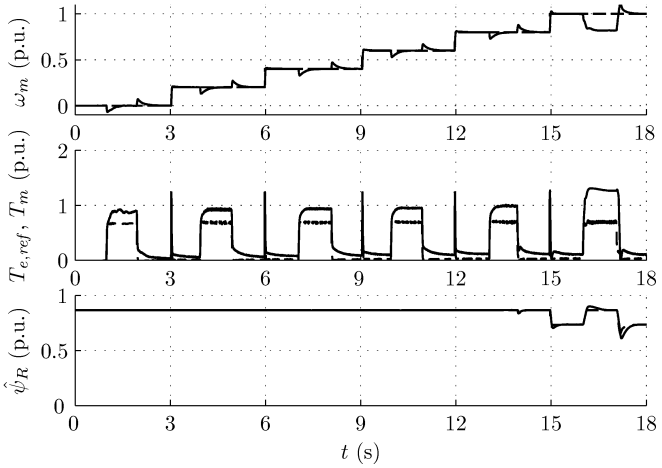

Fig. 11. Experimental results showing dynamic operation of the current model, $\hat{R}_R \approx 0.5R_R$. The first subplot shows the measured speed (solid) and the speed reference (dashed). The second subplot presents the torque reference (solid) and the measured shaft torque (dashed). The third subplot shows the magnitude of the estimated rotor flux (solid) and its reference (dashed).

becomes smaller, i.e., $\hat{L}_M > 0.75L_M$, thus reducing the torque error. The experiment could not be performed with $\hat{L}_M \approx 0.5L_M$. The produced torque became too large due to incorrect field orientation, and the braking resistor of the induction motor drive was not able to dissipate the energy produced in the field weakening region.

Fig. 10 shows the ratio of the reference torque to the measured shaft torque under erroneous parameters when the full-order flux observer is used. The results correspond well to the parameter sensitivity graphs in Fig. 5 except when the observer behaves like the approximate current model. The reasons for the differences are the same as explained earlier for the current model. Using the observer with the proposed gain, the experiment with $\hat{L}_M \approx 0.5L_M$ was possible since at higher speeds, the error in the produced torque was much smaller.

It is worth noting that the results of the parameter sensitivity graphs can be reproduced by controlling the slip to the value used in these graphs. In addition, the model of magnetic saturation of $\hat{L}_M$ is needed. This kind of simulations and experiments were carried out, and they showed excellent correspondence with the analytical results.

B. Dynamics

The dynamic behavior was studied using the speed mode control. Figs. 11 to 13 show experimental results obtained using erroneous parameter estimates. The speed reference was initially set to zero and it was increased every third second by a step of 0.2 p.u. until the speed 1 p.u. was achieved. Furthermore, using the loading machine, a rated load torque step (duration of one second) was applied every third second. The first load-torque step was applied at $t = 1$ s and the first speed reference step at $t = 3$ s. The reference torque $T_{e,ref}$ produced by the speed controller was compared to the measured shaft torque T_m.

Experimental results for the current model with $\hat{R}_R \approx 0.5R_R$ are shown in Fig. 11. During the load torque steps, there are large steady-state and dynamic errors between the

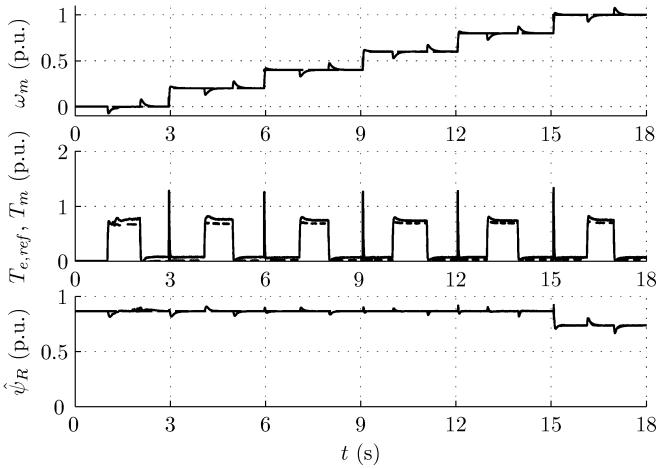

Fig. 12. Experimental results showing dynamic operation of the observer using the proposed gain, $\hat{R}_s \approx 0.5R_s$. The explanations of the curves are as in Fig. 11.

measured shaft torque and the reference torque. At low speeds, however, the speed controller forces the produced torque to equal the applied load torque. In the field-weakening, there is not enough voltage to be used due to incorrect flux estimation, and the speed cannot achieve its reference during $t = 16 \ldots 17$ s.

The observer using the proposed gain was used as the flux estimator in Figs. 12 and 13. Both the steady-state and dynamic errors between the measured torque and the reference torque are much smaller than in Fig. 11. The reference speed is achieved during the field weakening because of parameter insensitive flux estimation. It can also be noticed that a transition between the approximate current and voltage models is smooth.

High-speed operation under erroneous parameters is demonstrated in Fig. 14. The estimates of the resistances were $\hat{R}_s \approx 0.5R_s$ and $\hat{R}_R \approx 0.5R_R$. Furthermore, the estimate of the magnetizing inductance $\hat{L}_M$ was fixed to the base speed

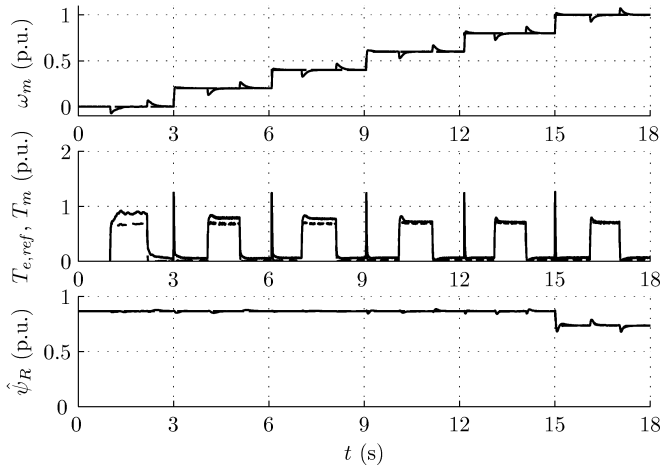

Fig. 13. Experimental results showing dynamic operation of the observer using the proposed gain, $\hat{R}_R \approx 0.5R_R$. The explanations of the curves are as in Fig. 11.

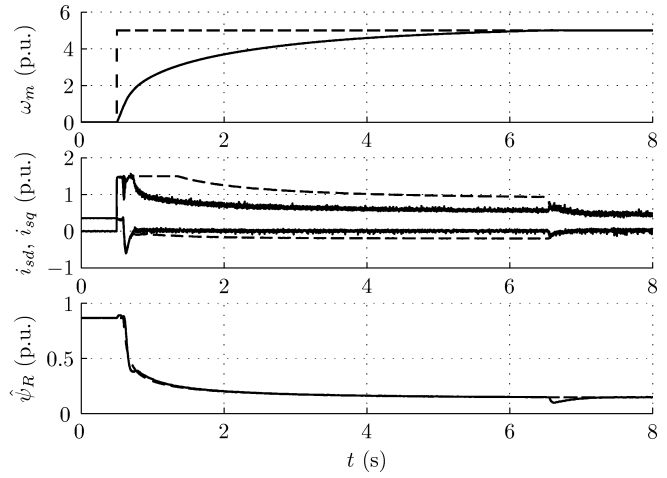

Fig. 14. Experimental results showing high-speed operation of the observer using the proposed gains, $\hat{R}_s \approx 0.5R_s$, $\hat{R}_R \approx 0.5R_R$, and constant $\hat{L}_M$ corresponding to the base speed region. The first subplot shows the measured speed (solid) and its reference (dashed). The second subplot shows the d and q components of the stator current (solid) and their references (dashed) in the estimated rotor flux reference frame. The third subplot presents the magnitude of the estimated rotor flux (solid) and its reference (dashed).

region value. During field weakening, there is a large error between the increased actual magnetizing inductance L_M (Fig. 9) and its constant-valued estimate $\hat{L}_M$. The speed reference was stepped from zero to 5 p.u. at $t = 0.5$ s. Since the PM servo acting as the loading machine cannot stand speeds above 2 p.u., it was replaced with an equal inertial mass in this experiment. The drive is operating in the overmodulation region even in the steady state due to high mechanical losses. It can be seen that high-speed operation is possible with highly erroneous motor parameters and without modelling the magnetic saturation. The noise in the current components originates from the overmodulation.

VIII. Conclusions

The parameter sensitivity of the full-order flux observers can be analyzed using analytical relations derived in the paper. The connection between the full-order flux observer and the current and voltage models was clarified. Based on the parameter sensitivity relations, practical methods of designing robust observer gains combining the current model and the voltage model are proposed. Parameter sensitivity studies both in the regeneration and motoring modes show that the desired combination of the current and voltage models was achieved. Proposed gains are easy to tune and lead to a simple structure of the observer.

Experimental results obtained using the observer with the proposed gain show that both the steady-state and dynamic errors in the produced torque under erroneous parameters are small as compared to the current model. Running out of the voltage at higher speeds (caused by the saturation of the motor due to inaccurate flux estimation) was not a problem. High-speed operation was possible with highly erroneous motor parameters and without modelling the magnetic saturation.

Appendix
Digital Implementation

The full-order flux observer discretized using the conventional forward Euler method becomes unstable at high speeds. The problem can be circumvented using two reference frames: the stator reference frame for the stator dynamics and the rotor reference frame for the rotor dynamics [14]. A simpler method is adopted here. The observer (4) is discretized as:

$$\hat{\psi}_{sd}^{k+1} = \hat{\psi}_{sd}^{k} + T_s\Big(-\tfrac{1}{\hat{\tau}_s}\hat{\psi}_{sd}^{k} + \hat{\omega}_s^{k}\hat{\psi}_{sq}^{k} + \tfrac{1}{\hat{\tau}_s'}\hat{\psi}_R^{k} + u_{sd}^{k} + l_{sd}\tilde{i}_{sd}^{k} - l_{sq}\tilde{i}_{sq}^{k}\Big) \tag{17a}$$

$$\hat{\psi}_{sq}^{k+1} = \hat{\psi}_{sq}^{k} + T_s\Big(-\hat{\omega}_s^{k}\hat{\psi}_{sd}^{k+1} - \tfrac{1}{\hat{\tau}_s'}\hat{\psi}_{sq}^{k} + u_{sq}^{k} + l_{sd}\tilde{i}_{sq}^{k} + l_{sq}\tilde{i}_{sd}^{k}\Big) \tag{17b}$$

$$\hat{\psi}_R^{k+1} = \hat{\psi}_R^{k} + T_s\Big(\tfrac{1-\hat{\sigma}}{\hat{\tau}_r'}\hat{\psi}_{sd}^{k+1} - \tfrac{1}{\hat{\tau}_r'}\hat{\psi}_R^{k} + l_{rd}\tilde{i}_{sd}^{k} - l_{rq}\tilde{i}_{sq}^{k}\Big) \tag{17c}$$

$$\hat{\omega}_s^{k+1} = \omega_m^{k} + \frac{\frac{1-\hat{\sigma}}{\hat{\tau}_r'}\hat{\psi}_{sq}^{k+1} + l_{rd}\tilde{i}_{sq}^{k} + l_{rq}\tilde{i}_{sd}^{k}}{\hat{\psi}_R^{k+1}} \tag{17d}$$

where T_s is the sampling period. In contrast to the forward Euler method, the new values of the states are used when available (except in the current errors for simplicity). This method has similarities with [15] and it can be seen as a mixture of the forward Euler and backward Euler methods. Contrary to the forward Euler method, the old values of the updated states need not to be preserved and the implementation becomes simpler. Computer simulations with observer gains giving different eigenvalues indicate that the stability region of the method suits well for full-order flux observers. No problems were encountered even at very high speeds (see also Fig. 14).

Acknowledgment

This work was financed in part by ABB Oy.

REFERENCES

[1] R. Krishnan and F. C. Doran, "Study of parameter sensitivity in high-performance inverter-fed induction motor drive systems," *IEEE Trans. Ind. Applicat.*, vol. IA-23, no. 4, pp. 623–635, July/Aug. 1987.

[2] P. L. Jansen and R. D. Lorenz, "A physically insightful approach to the design and accuracy assessment of flux observers for field oriented induction machine drives," *IEEE Trans. Ind. Applicat.*, vol. 30, no. 1, pp. 101–110, Jan./Feb. 1994.

[3] G. C. Verghese and S. R. Sanders, "Observers for flux estimation in induction machines," *IEEE Trans. Ind. Electron.*, vol. 35, no. 1, pp. 85–94, Feb. 1988.

[4] H. Kubota, K. Matsuse, and T. Nakano, "DSP-based speed adaptive flux observer of induction motor," *IEEE Trans. Ind. Applicat.*, vol. 29, no. 2, pp. 344–348, Mar./Apr. 1993.

[5] J. Maes and J. A. Melkebeek, "Speed-sensorless direct torque control of induction motors using an adaptive flux observer," *IEEE Trans. Ind. Applicat.*, vol. 36, no. 3, pp. 778–785, May/June 2000.

[6] L. Harnefors, "Design and analysis of general rotor-flux-oriented vector control systems," *IEEE Trans. Ind. Electron.*, vol. 48, no. 2, pp. 383–390, Apr. 2001.

[7] B. Peterson, "Induction machine speed estimation – observations on observers," Ph.D. dissertation, Department of Industrial Electrical Engineering and Automation, Lund University, Lund, Sweden, Feb. 1996.

[8] L. Harnefors, "On analysis, control and estimation of variable-speed drives," Ph.D. dissertation, Electrical Machines and Drives, Department of Electric Power Engineering, Royal Institute of Technology, Stockholm, Sweden, Oct. 1997.

[9] B. Robyns, F. Berthereau, G. Cossart, L. Chevalier, F. Labrique, and H. Buyse, "A methodology to determine gains of induction motor flux observers based on a theoretical parameter sensitivity analysis," *IEEE Trans. Power Electron.*, vol. 15, no. 6, pp. 983–995, Nov. 2000.

[10] H. Hofmann and S. R. Sanders, "Speed-sensorless vector torque control of induction machines using a two-time-scale approach," *IEEE Trans. Ind. Applicat.*, vol. 34, no. 1, pp. 169–177, Jan./Feb. 1998.

[11] L. Harnefors and H.-P. Nee, "Model-based current control of AC machines using the internal model control method," *IEEE Trans. Ind. Applicat.*, vol. 34, no. 1, pp. 133–141, Jan./Feb. 1998.

[12] F. Briz, M. W. Degner, and R. D. Lorenz, "Analysis and design of current regulators using complex vectors," *IEEE Trans. Ind. Applicat.*, vol. 36, no. 3, pp. 817–825, May/June 2000.

[13] F. Briz, A. Diez, M. W. Degner, and R. D. Lorenz, "Current and flux regulation in field-weakening operation [of induction motors]," *IEEE Trans. Ind. Applicat.*, vol. 37, no. 1, pp. 42–50, Jan./Feb. 2001.

[14] M. Hinkkanen and J. Luomi, "Digital implementation of full-order flux observers for induction motors," in *Proc. EPE-PEMC'02*, Cavtat & Dubrovnik, Croatia, Sept. 2002.

[15] J. Niiranen, "Fast and accurate symmetric Euler algorithm for electromechanical simulations," in *Proc. Elecrimacs'99*, vol. 1, Lisboa, Portugal, Sept. 1999, pp. 71–78.

Marko Hinkkanen was born in Rautjarvi, Finland, in 1975. He received the M.Sc. degree in electrical engineering in 2000 from Helsinki University of Technology, Espoo, Finland, where he is currently working toward the D.Sc. degree.

Since 2000, he has been with the Power Electronics Laboratory, Helsinki University of Technology, as a research scientist. His main research interest is the control of electrical drives.

Jorma Luomi was born in Helsinki, Finland, in 1954. He received his M.Sc. (Eng.) and D.Sc. (Tech.) degrees from Helsinki University of Technology in 1977 and 1984, respectively.

In 1980 he joined Helsinki University of Technology, and from 1991 to 1998 he was a Professor at Chalmers University of Technology. As of 1998 he holds the position of Professor at the Department of Electrical and Communications Engineering at Helsinki University of Technology. His research interests are in the areas of electric drives, electric machines and numerical analysis of electromagnetic fields.